Collective Dipole Oscillations of a Spin-Orbit Coupled Bose-Einstein Condensate

Jin-Yi Zhang,[1] Si-Cong Ji,[1] Zhu Chen,[2] Long Zhang,[1] Zhi-Dong Du,[1] Bo Yan,[1] Ge-Sheng Pan,[1] Bo Zhao,[1] You-Jin Deng,[1,*] Hui Zhai,[2,†] Shuai Chen,[1,‡] and Jian-Wei Pan[1,§]

[1]*Hefei National Laboratory for Physical Sciences at Microscale and Department of Modern Physics, University of Science and Technology of China, Hefei, Anhui 230027, People's Republic of China*
[2]*Institute for Advanced Study, Tsinghua University, Beijing 100084, China*

(Received 14 March 2012; revised manuscript received 3 July 2012; published 12 September 2012)

In this Letter, we present an experimental study of the collective dipole oscillation of a spin-orbit coupled Bose-Einstein condensate in a harmonic trap. The dynamics of the center-of-mass dipole oscillation is studied in a broad parameter region as a function of spin-orbit coupling parameters as well as the oscillation amplitude. The anharmonic properties beyond the effective-mass approximation are revealed, such as the amplitude-dependent frequency and finite oscillation frequency at a place with a divergent effective mass. These anharmonic behaviors agree quantitatively with variational wave-function calculations. Moreover, we experimentally demonstrate a unique feature of the spin-orbit coupled system predicted by a sum-rule approach, stating that spin polarization susceptibility—a static physical quantity—can be measured via the dynamics of dipole oscillation. The divergence of polarization susceptibility is observed at the quantum phase transition that separates the magnetic nonzero-momentum condensate from the nonmagnetic zero-momentum phase. The good agreement between the experimental and theoretical results provides a benchmark for recently developed theoretical approaches.

DOI: 10.1103/PhysRevLett.109.115301 PACS numbers: 67.85.De, 03.75.Kk, 67.85.Fg

Many interesting quantum phases can emerge in solid-state materials when electrons are placed in a strong magnetic field or possess strong spin-orbit (SO) coupling, such as the fractional quantum Hall effect [1] and the topological insulator [2]. In cold atom systems, albeit neutral atoms have neither charges nor SO coupling, the recent exciting experimental progress demonstrates that artificial gauge potentials can by synthesized in a laboratory by a laser control technique [3–10]. The synthetic gauge potential is becoming a powerful tool for simulating real materials with cold atoms. Moreover, the system of SO-coupled bosons does not have an analogy in conventional condensed matter systems, and can exhibit many novel phases [11] such as the striped superfluid phase [12,13] and the half vortex phase [14–17].

Collective excitations play an important role in studying the physical properties of trapped atomic Bose-Einstein condensates (BEC) and degenerate Fermi gases. Collective dipole oscillation is a center-of-mass motion of all atoms. For a conventional condensate, dipole oscillation is trivial: the frequency is just the harmonic-trap frequency, independent of oscillation amplitude and interatomic interaction. This is known as the Kohn theorem [18,19]. For a SO-coupled condensate, however, it was found [4] that the dipole-oscillation frequency deviates from the trap frequency, and therefore the experimental data can be explained by effective-mass approximation. Recently, much theoretical effort has been taken to understand the dynamics of a SO-coupled BEC [20–25], and many predicted unconventional properties remain to be experimentally explored. In particular, the so-called sum-rule approach predicts [25] a unique feature of SO-coupled condensates: spin polarization susceptibility—a static physical quantity—can be measured via the dynamics of dipole oscillation.

In this Letter, we experimentally study the collective dipole oscillation of a SO-coupled ^{87}Rb BEC that occurs both in momentum and magnetization. The oscillation frequency is measured along various paths in the phase diagram as a function of the SO-coupling parameters and oscillation amplitude. Anharmonic properties beyond the effective-mass approximation are observed, including the amplitude-dependent frequency and finite oscillation frequency at places with infinite effective mass. The experimental data fit well with variational wave-function calculations. Moreover, following a proposal of the sum-rule approach [25], we deduce the spin polarization susceptibility from the amplitude ratio between the momentum and magnetization oscillations; the results are in good agreement with theoretical calculations. In particular, the measured spin polarization susceptibility does diverge at the quantum phase transition that separates the magnetic nonzero-momentum condensate from the nonmagnetic zero-momentum phase.

The experimental layout is sketched in Fig. 1(a). A ^{87}Rb BEC of about 2.5×10^5 atoms is produced in the crossed optical dipole trap with wavelength 1070 nm, beam waist 80 μm, and trap frequency $\omega = 2\pi \times \{45, 45, 55\}$ Hz. A bias magnetic field $\mathbf{B}_{\text{bias}}$ is applied in the z direction. The BEC is illuminated by a pair of Raman lasers in the x-y plane with beam waist 240 μm, relative angle $\theta = 105°$, and wavelength $\lambda = 803.3$ nm. The Raman lasers couple

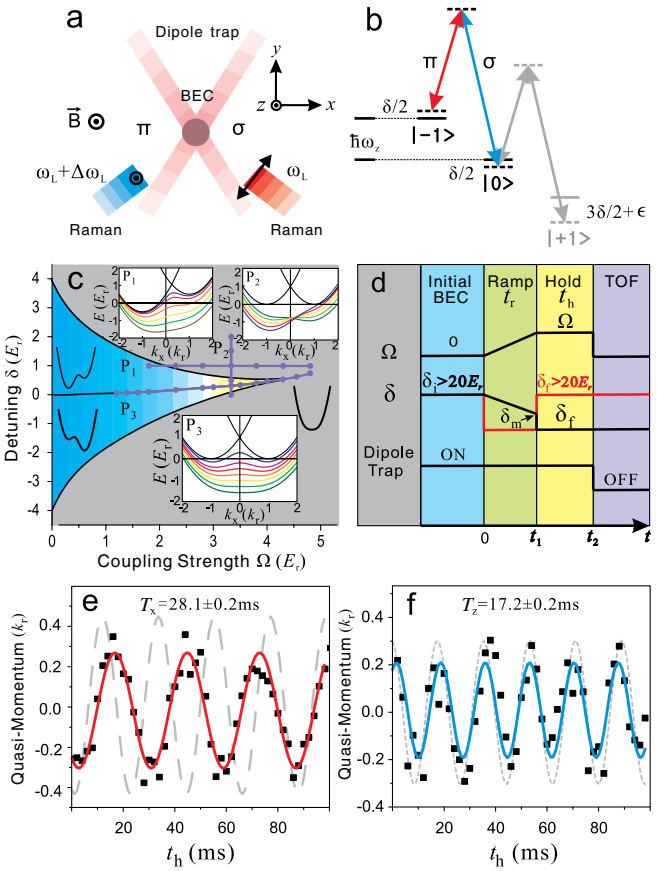

FIG. 1 (color online). (a) Experimental layout. The field $\mathbf{B}_{\text{bias}}$ is along the z direction and the Raman lasers propagate in the x-y plane. (b) Raman coupling scheme within the $F = 1$ manifold. (c) Single-particle phase diagram in the Ω-δ plane. The dispersion spectrum $\mathcal{E}(k_x)$ has two (one) local minima in the blue (grey) regime. The experiments are along the paths P_1, P_2, and P_3, with $\mathcal{E}(k_x)$ in the insets. (d) Experimental time sequence. (e–f) Dipole oscillation with $\Omega = 3.3E_r$ and $\delta = 1E_r$ along the $\hat{x}(e)$ and $\hat{z}$ (f) directions. For comparison, the oscillations without SO coupling are displayed as grey dashed curves.

the three internal states of the $F = 1$ manifold, as shown in Fig. 1(b). By setting the quadratic Zeeman shift $\epsilon = 3.37E_r$ with recoil energy $E_r = k_r^2/(2m) = 2\pi \times 2.21$ kHz (k_r is the recoil momentum), we effectively suppress the state $|m_{\text{F}} = 1\rangle$ and prepare a spin-1/2 system by regarding the state $|m_{\text{F}} = -1\rangle$ as $|\uparrow\rangle$ and $|m_{\text{F}} = 0\rangle$ as $|\downarrow\rangle$. This leads to a single-particle Hamiltonian as ($\hbar = 1$)

$$\hat{H}_0 = \begin{pmatrix} \frac{(k_x+k_r)^2}{2m} - \frac{\delta}{2} & \frac{\Omega}{2} \\ \frac{\Omega}{2} & \frac{(k_x-k_r)^2}{2m} + \frac{\delta}{2} \end{pmatrix}, \quad (1)$$

where k_x is the quasimomentum, Ω is the strength of Raman coupling, and δ is the two-photon Raman detuning. The diagonalization of Eq. (1) yields two eigenstates for each k_x, in which the spin and the momentum of an atom are coupled. For a small Ω and δ, energy dispersion $\mathcal{E}(k_x)$ has two local minima, and bosons condense in one of the minima for our current experimental conditions. For a large Ω or δ, energy dispersion $\mathcal{E}(k_x)$ has only one minimum. The phase boundary between the double- and single-minimum region is displayed in Fig. 1(c), in which the perturbative effect of state $|m_{\text{F}} = 1\rangle$ has been taken into account (as well as in theoretical calculations later). We shall systematically study the dipole oscillations along the paths P_1, P_2, and P_3 in Fig. 1(c).

The time sequence for the experiment is shown in Fig. 1(d). After the BEC is prepared in the trap ($t = 0$), Raman coupling is adiabatically ramped up from zero to Ω in a time period t_1 from 70 to 100 ms, and $\mathbf{B}_{\text{bias}}$ is slowly ramped, which adiabatically changes δ from an initial value of $\delta_i > 20E_r$ to an intermediate value of δ_m. At t_1, detuning δ is switched from δ_m to δ_f [black line in Fig. 1(d)] in 1 ms, which is much faster than the oscillation period but slow enough for the BEC to remain in the lower eigenstate. This process effectively gives the BEC a pulsed momentum, named synthetic electric force in Ref. [4]. Further, by varying δ_m, one excites the dipole oscillation with different amplitudes. The BEC starts to oscillate at t_1 and is held for a holding time $t_h = t_2 - t_1$. At t_2, both the Raman lasers and the trap are quickly switched off within 1 ms. With the Stern-Gerlach technique, a time-of-flight (TOF) image is taken after 24 ms of free expansion to map out the spin and momentum of the BEC. A comparison experiment without SO coupling is also carried out by setting a large detuning $\delta > 20E_r$ instead of turning off the Raman lasers. Accordingly, the time sequence for $\mathbf{B}_{\text{bias}}$ is modified: $\mathbf{B}_{\text{bias}}$ is initially set for $\delta = \delta_f$ at $t = 0$ and quickly switched to be $\delta > 20E_r$ at t_2 [red line in Fig. 1(d)].

Momentum oscillation.—Figures 1(e) and 1(f) display the typical momentum oscillations observed in the experiment. The frequency along $\hat{x}$ is significantly changed by SO coupling, while those along $\hat{y}$ and $\hat{z}$ remain to be the trap frequency (independent of oscillation amplitude). Figure 2(a) shows the oscillation period T_x versus Ω along the path P_1 ($\delta = 1E_r$). As Ω increases, the deviation from the trap frequency becomes larger. Moreover, it is found that T_x is amplitude dependent, as shown in Fig. 2(b) for $\Omega = 4.8E_r$ and $\delta = 1E_r$. These two features clearly demonstrate that the dipole oscillation along the x direction is no longer harmonic.

Similar Ω dependence of T_x along P_2 and P_3 are displayed in Figs. 2(c) and 2(d). In the yellow regime of Fig. 1(c), the single-particle spectrum has two nearly degenerate minima, separated by a barrier as low as trapping energy. In this regime, the dipole oscillation becomes rather complicated and does not fit a single-frequency oscillation [shown in the inset of Fig. 2(d)].

This anharmonic behavior can be understood from the equation of motion. Consider Hamiltonian $\hat{H} = \sum_i (H_{0,i} + (1/2)m\omega_\alpha^2 r_{\alpha i}^2) + \sum_{i<j} U(\mathbf{r}_i - \mathbf{r}_j)$, where α sums over x, y, and z, and $U(\mathbf{r})$ represents two-body interactions. Let $\hat{X}$: $\equiv (1/N)\sum_i x_i$ be the center-of-mass

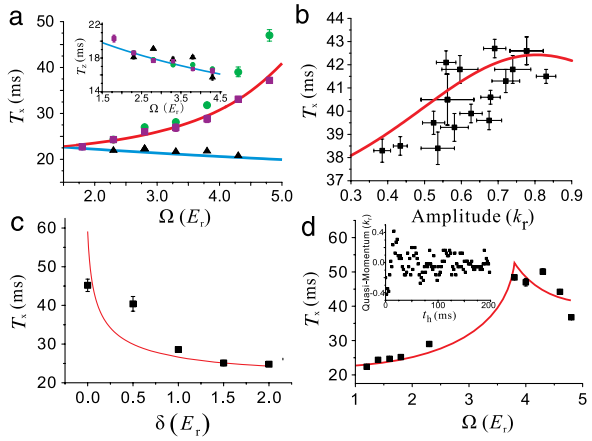

FIG. 2 (color online). (a) Oscillation period T_x along path P_1 ($\delta = 1E_r$) versus Ω. The black triangles are without SO coupling, and the blue line denotes the estimated trap frequency. The purple squares are with SO coupling for relatively small (below $0.2k_r$) oscillation amplitude, while the green circles are for large (about $0.6k_r$) amplitude. The inset is for T_z versus Ω. (b) T_x versus oscillation amplitude with ($\Omega = 4.8, \delta = 1.0)E_r$. The black squares with error bars are experimental data. (c) and (d) T_x versus Ω along path P_2 and path P_3. In all plots, the red lines are the theory curves obtained by solving Eq. (2).

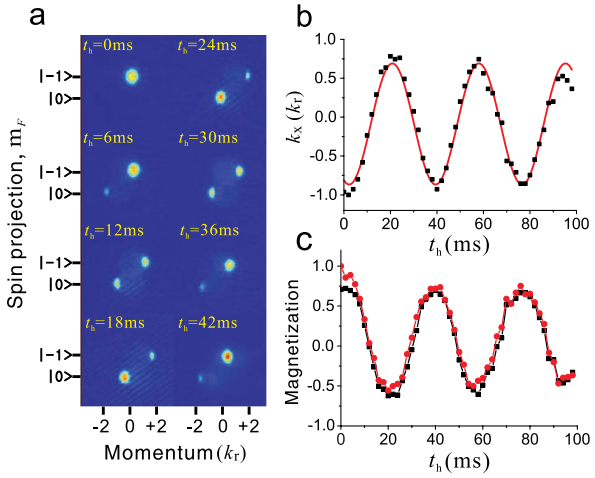

FIG. 3 (color online). Magnetization oscillation for $\delta = 1E_r$ and $\Omega = 4.8E_r$. (a) Spin-resolved TOF images for various holding times t_h. (b) Quasimomentum k_x versus t_h. (c) Polarization $\mathcal{M}$ versus t_h. The red circles are directly measured, while the black squares are deduced from (b) (see text for details).

displacement operator (N being the number of atoms); then the equation of motion for X can be derived as $\dot{\hat{X}} = 1/(Nm)\sum_i(\hat{k}_{x,i} + k_r\sigma_{z,i})$ and $\ddot{\hat{X}} = -\omega_x^2\hat{X} + i\Omega k_r\sum_i\sigma_{y,i}$. For either the conditions of no coupling between spins ($\Omega = 0$) or momentum-independent coupling, e.g., coupled by radio-frequency field with $k_r = 0$, the equation of motion will close at the second order, yielding harmonic oscillation and the well-known Kohn theorem [18,19]. For both nonzero Ω and k_r, however, the equation of motion cannot close at any finite order. This results in anharmonic dipole oscillation.

For a quantitative calculation of the oscillation frequency, we shall use a variational wave-function approach [26]. We first assume that the condensate stays in the lower eigenbranch during the entire oscillation [24]. We further ignore spin-dependent interactions, because the spin-dependent interaction energy is about 0.46% of the total energy for the $F = 1$ manifold of ^{87}Rb atoms [27], and the aspect ratio of condensate in our experiments is far from "mode resonance" [24]. With these simplifications, the dipole oscillation is described by [24]

$$\dot{k}_x = -\omega_x^2 x, \qquad \dot{x} = \partial\mathcal{E}(k_x)/\partial k_x. \tag{2}$$

As shown in Fig. 2, our experimental data agree well with the calculations based on Eq. (2). In particular, for ($\Omega = 4E_r$, $\delta = 0$), where the effective-mass approximation breaks down because of the divergent effective mass, Fig. 2 shows that the oscillation frequency remains finite.

Magnetization oscillation.—The Stern-Gerlach TOF images in Fig. 3(a) show that during dipole oscillation, the spin population also oscillates. Figures 3(b) and 3(c) display the oscillation of quasimomentum k_x and polarization $\mathcal{M} = (n_\uparrow - n_\downarrow)/(n_\uparrow + n_\downarrow)$, respectively; it can be seen that the oscillation frequencies are exactly identical. To provide an intuitive picture, we assume that during the entire oscillation, the BEC remains at the lower eigenstate branch of Hamiltonian Eq. (1), and the spin configuration adiabatically follows the center-of-mass motion. The eigenstate wave function of the lower branch $\psi = f_\uparrow(k_x)|\uparrow\rangle + f_\downarrow(k_x)|\downarrow\rangle$ can be obtained by diagonalizing Eq. (1), which yields $\mathcal{M}(k_x) = |f_\uparrow(k_x)|^2 - |f_\downarrow(k_x)|^2$. Hence, the magnetization changes with k_x. The function $\mathcal{M}(t)$ can be then obtained by using the experimentally measured $k_x(t)$ [Fig. 3(b)]. The results are shown as black squares in Fig. 3(c), and agree very well with the directly measured data (red circles). The magnetization oscillation reflects the locking between the spin and momentum in the Hamiltonian Eq. (1) and further provides a direct justification for the assumption in the variational wave-function approach.

Magnetization oscillation can be understood from the absence of Galilean invariance. Consider a BEC that moves with a velocity v along $\hat{x}$; in the comoving frame, the single-particle Hamiltonian acquires an additional term vk_x. In a conventional BEC, this term can be gauged away by a gauge transformation $\psi \rightarrow e^{imvx}\psi$. In our system, however, such a procedure will introduce a velocity-dependent Zeeman-energy term $-mvk_r\sigma_z$. Hence, once the condensate moves, an oscillation of magnetization $\mathcal{M}$ has to be induced.

Spin polarization susceptibility and quantum phase transition.—A unique feature of a SO-coupled condensate is that spin polarization susceptibility can be deduced from

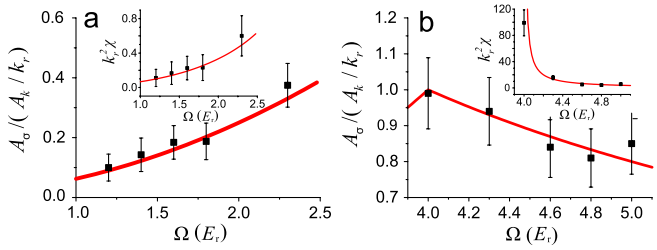

FIG. 4 (color online). Amplitude ratio of spin and momentum oscillation $A_\sigma/(A_k/k_r)$ versus Ω, for magnetic phase (a) and nonmagnetic phase (b). The inset is for the spin polarization susceptibility $E_r\chi$ deduced from this ratio via Eq. (4). The red solid line is from the solution of Eq. (3).

the amplitude ratio between the momentum and magnetization oscillations [25]. Here, we focus on $\delta = 0$. For $\Omega < 4E_r$, the bosons condense in one of the double minima, which spontaneously breaks the time-reversal symmetry and has nonzero magnetization $\langle\sigma_z\rangle$. For $\Omega > 4E_r$, the bosons condense in the zero-momentum state with zero magnetization. Thus, there is a phase transition from the magnetic condensate to the nonmagnetic condensate state as Ω varies [23,25]. The spin polarization susceptibility χ can then be expressed as [25]

$$\chi = \begin{cases} \frac{\Omega^2/2E_r}{16E_r^2-\Omega^2} & \text{for } \Omega < 4E_r \\ \frac{2}{\Omega-4E_r} & \text{for } \Omega > 4E_r \end{cases}. \tag{3}$$

Equation (3) predicts that χ diverges at the phase transition point $\Omega = 4E_r$. It is further proposed [25] that χ can be measured from the amplitude ratio between the spin and momentum oscillations via

$$\frac{A_\sigma}{A_k/k_r} = \frac{E_r\chi}{1+E_r\chi}. \tag{4}$$

We experimentally measure the ratio $A_\sigma/(A_k/k_r)$ and compare the data with the theoretical prediction by Eq. (3). Figures 4(a) and 4(b) show the results for the magnetic phase with $\Omega < 2.5E_r$ and the nonmagnetic phase with $\Omega > 4E_r$, respectively. Note that for the reason discussed above, no experimental data are available for $2.5E_r < \Omega < 4E_r$. We further deduce the susceptibility χ via Eq. (4) from the experimental ratio $A_\sigma/(A_k/k_r)$, shown in the inset of Fig. 4. The excellent agreement with the theoretical results confirm the unique features of the SO-coupled condensate whose spin susceptibility can be measured via dipole oscillation. In particular, one can find that as $\Omega \to 4E_r + 0^+$, χ does display divergent behavior, giving strong evidence of quantum phase transition.

In summary, we have experimentally demonstrated nontrivial properties of the dipole oscillation for a SO-coupled BEC. From the experimentally measured dynamics of dipole oscillation, we further display the divergent behavior of spin polarization susceptibility—a static physical quantity—at the quantum phase transition. Besides being a direct experimental observation of unconventional dynamics in a SO-coupled condensate, our quantitative results also provide a benchmark for various recently developed theoretical approaches. It is expected that the further study of dynamic behavior would provide a powerful tool in probing novel phases of SO-coupled BEC, such as the stripe superfluid phase [12,13].

H. Z. would like to thank Sandro Stringari and Lev Pitaevskii for valuable discussions. The measurement of spin polarization susceptibility via Eq. (4) was suggested by Sandro Stringari. This work has been supported by the NNSF of China, the CAS, the National Fundamental Research Program (under Grants No. 2011CB921300 and No. 2011CB921500), and NSERC.

*yjdeng@ustc.edu.cn
†hzhai@mail.tsinghua.edu.cn
‡shuai@ustc.edu.cn
§pan@ustc.edu.cn

[1] D. C. Tsui, H. L. Stormer, and A. C. Gossard, Phys. Rev. Lett. **48**, 1559 (1982).
[2] M. Z. Hasan and C. L. Kane, Rev. Mod. Phys. **82**, 3045 (2010); X.-L. Qi and S.-C. Zhang, Rev. Mod. Phys. **83**, 1057 (2011).
[3] Y.-J. Lin, R. L. Compton, A. R. Perry, W. D. Phillips, J. V. Porto, and I. B. Spielman, Phys. Rev. Lett. **102**, 130401 (2009); Y.-J. Lin, R. L. Compton, K. Jiménez-García, J. V. Porto, and I. B. Spielman, Nature (London) **462**, 628 (2009).
[4] Y.-J. Lin, R. L. Compton, K. Jiménez-García, W. D. Phillips, J. V. Porto, and I. B. Spielman, Nature Phys. **7**, 531 (2011).
[5] Y.-J. Lin, K. Jiménez-García, and I. B. Spielman, Nature (London) **471**, 83 (2011).
[6] R. A. Williams, L. J. LeBlanc, K. Jiménez-García, M. C. Beeler, A. R. Perry, W. D. Phillips, and I. B. Spielman, Science **335**, 314 (2011).
[7] M. Aidelsburger, M. Atala, S. Nascimbène, S. Trotzky, Y.-A. Chen, and I. Bloch, Phys. Rev. Lett. **107**, 255301 (2011).
[8] Z. Fu, P. Wang, S. Chai, L. Huang, and J. Zhang, Phys. Rev. A **84**, 043609 (2011).
[9] P. Wang, Z.-Q. Yu, Z. Fu, J. Miao, L. Huang, S. Chai, H. Zhai, and J. Zhang, Phys. Rev. Lett. **109**, 095301 (2012).
[10] L. W. Cheuk, A. T. Sommer, Z. Hadzibabic, T. Yefsah, W. S. Bakr, and M. W. Zwierlein, Phys. Rev. Lett. **109**, 095302 (2012).
[11] H. Zhai, Int. J. Mod. Phys. B **26**, 1230001 (2012).
[12] C. Wang, C. Gao, C.-M. Jian, and H. Zhai, Phys. Rev. Lett. **105**, 160403 (2010).
[13] T.-L. Ho and S. Zhang, Phys. Rev. Lett. **107**, 150403 (2011).
[14] C.-J. Wu, I. Mondragon-Shem, and X.-F. Zhou, Chin. Phys. Lett. **28**, 097102 (2011).
[15] T. D. Stanescu, B. Anderson, and V. Galitski, Phys. Rev. A **78**, 023616 (2008).
[16] H. Hu, B. Ramachandhran, H. Pu, and X.-J. Liu, Phys. Rev. Lett. **108**, 010402 (2012).

[17] S. Sinha, R. Nath, and L. Santos, Phys. Rev. Lett. **107**, 270401 (2011).
[18] S. Stringari, Phys. Rev. Lett. **77**, 2360 (1996).
[19] W. Kohn, Phys. Rev. **123**, 1242 (1961); F. Dalfovo, S. Giorgini, L. P. Pitaevskii, and S. Stringari, Rev. Mod. Phys. **71**, 463 (1999).
[20] E. van der Bijl and R. A. Duine, Phys. Rev. Lett. **107**, 195302 (2011).
[21] B. Ramachandhran, B. Opanchuk, X.-J. Liu, H. Pu, P. D. Drummond, and H. Hu, Phys. Rev. A **85**, 023606 (2012).
[22] Y. Zhang, L. Mao, and C. Zhang, Phys. Rev. Lett. **108**, 035302 (2012).
[23] Y. Zhang, G. Chan, and C. Zhang, arXiv:1111.4778.
[24] Z. Chen and H. Zhai, arXiv:1204.5121.
[25] Y. Li, G. Martone and S. Stringari, arXiv:1205.6398.
[26] V. M. Pérez-García, H. Michinel, J. I. Cirac, M. Lewenstein, and P. Zoller, Phys. Rev. Lett. **77**, 5320 (1996).
[27] A. Widera, F. Gerbier, S. Fölling, T. Gericke, O. Mandel, and I. Bloch, New J. Phys. **8**, 152 (2006).